

Article

Quantitative Assessment of Cold Injury in Tea Plants by Terahertz Spectroscopy Method

Yongzong Lu ^{1,2} , Eric Amoah Asante ³, Hongwei Duan ⁴ and Yongguang Hu ^{1,*}¹ School of Agricultural Engineering, Jiangsu University, Zhenjiang 212013, China; yzlu@ujs.edu.cn² Jiangsu LINHAI Group, Taizhou 225310, China³ Department of Agricultural and Biosystems Engineering, Kwame Nkrumah University of Science and Technology, Kumasi AK-039-5028, Ghana; ericasante@knust.edu.gh⁴ College of Mechanical and Electrical Engineering, Shihezi University, Shihezi 832003, China; dhwsg123@shzu.edu.cn

* Correspondence: deerhu@ujs.edu.cn

Abstract: Cold injury (CI) causes irreversible damage to tea plants, which results in decline in the quality of famous teas and huge economic loss. A new, quick, non-destructive method is provided to assess the CI of tea leaf based on terahertz (THz) spectroscopy. Absorbance of the samples was measured with THz spectroscopy in frequency bands from 0.1 to 1.6 THz under low temperature treatments of 4.0, 0, −2.5, −5.0, −7.5, and −10.0 °C. Fast Fourier transformation was explored to decompose the endpoint signal to improve the ratio of signal to air and convert the time-domain spectra to the corresponding frequency-domain spectra. To improve the separation of overlap signals caused by substantial scattering of injured cells in the leaf, two-dimensional correlation spectroscopy (2DCOS) and average intensity (AI) were introduced into the partial least squares regression (PLSR) to build 2DCOS–PLSR and AI–PLSR models. Quantitative assessments of the 2DCOS–PLSR and AI–PLSR models were conducted to evaluate the three models. The assessment results showed that the correlation coefficients of the 2DCOS–PLSR model (R_{2D}) were 0.7873, 0.8305, and 0.9103, respectively. The root mean square errors of the 2DCOS–PLSR model ($RMSE_{2D}$) were 0.6032, 0.5763, and 0.5221, respectively. For the AI–PLSR model, R_{AI} values were 0.7477, 0.7691, and 0.8974, respectively. $RMSE_{AI}$ values were 0.6038, 0.5962, and 0.5797. The combination of THz spectroscopy with the 2DCOS–PLSR model provided a better benchmark for the input interval selection and improved the accuracy of cold-injury detection results.

Keywords: cold injury; terahertz spectroscopy; two-dimensional correlation spectroscopy; absorbance; signal processing



Citation: Lu, Y.; Asante, E.A.; Duan, H.; Hu, Y. Quantitative Assessment of Cold Injury in Tea Plants by Terahertz Spectroscopy Method. *Agronomy* **2023**, *13*, 1376. <https://doi.org/10.3390/agronomy13051376>

Academic Editors: Lorena Parra and Laura García

Received: 23 April 2023

Revised: 11 May 2023

Accepted: 13 May 2023

Published: 15 May 2023



Copyright: © 2023 by the authors. Licensee MDPI, Basel, Switzerland. This article is an open access article distributed under the terms and conditions of the Creative Commons Attribution (CC BY) license (<https://creativecommons.org/licenses/by/4.0/>).

1. Introduction

Tea (*Camellia sinensis*) is one of the most common materials for food and beverages in the world due to its health benefits for human consumption [1,2]. The tea plant is mainly grown in humid and warm hilly areas, where survival is mainly restricted by freezing temperatures in the late spring [3–5]. In China, the plant has been suffering from cold injury (CI) over the past decades, leading to a decline in production and huge economic losses [6–9]. The freezing events that occur during winter are usually not the only critical risks to the cold survival of tea [10], so the extent of tolerance is crucial [11,12]. However, severe physiological damage to the plant can take place when it is exposed to freezing temperatures for a long period. Furthermore, CI can decrease the efficiency of the nutrient transmission from the roots to the leaves [13,14]. Therefore, the search for cold-tolerant cultivars could revolve around the differences in their ability to survive long-term freezing [15,16]. Many available cold-resistance data have been determined on detached plant material before freezing. However, in the plant's environment, the whole plant is exposed to the freezing temperature, which means that in situ cold resistance assessment is

required [10]. Therefore, cold injury assessment of several leaves on a living plant under cumulative decreases in temperature is the best for optimal conclusions [17].

Recently, various techniques have been developed to monitor and determine the degree of CI in plants. These can be divided into destructive and non-destructive techniques [18]. The destructive techniques, some of which involve clamping, can damage the leaf depending on the clamping force and the clamping duration, which may render the data acquired defective. Moreover, those methods are time consuming and are also not suitable for on-line detection [19]. Thus, a more effective and non-destructive approach is required for CI detection [20]. One of the emerging non-destructive techniques, terahertz (THz) time-domain spectroscopy, has been widely explored in field research in food and agricultural products [21]. For detection-related research in food and agricultural products, the frequency range of 0.1–1.6 THz is very sensitive [22,23], so the THz spectroscopy technique offers better spatial resolution due to its smaller wavelength [24].

THz spectroscopy has also been extended into investigating stress in plant leaves. Jördens et al. [18] investigated the permittivity of coffee leaves at THz frequencies and reported that the dielectric material parameters can be used to determine the leaf water status. The technique was similarly applied in a water stress assessment, with the water content variation in the leaf affecting its thickness, which was reflected in the THz absorption spectral values. Moreover, there is a direct correlation between the freezing temperature and the amount of water that escapes out of the leaf due to cell damage [24]. The differences in the degree of cell opening at different locations in the leaf during freezing require single-point measurements over the entire leaf surface. The measured average presents data that fairly represent the CI of the leaf. The degree of CI and the resistance to low temperatures can be reflected in the spectral differences [25–30], because the freezing temperature causes a higher degree of cell opening, resulting in a larger quantity of water oozing out. It is also well established that THz radiation is strongly absorbed by water and that the total absorption depends on the optical-path length through which the wave is transmitted [31,32]. A decrease in the leaf water content has a direct correlation with an increase in THz transmission, because water is opaque in the THz band [33,34]. Similarly, when a plant suffers from severe CI, the path length of the water will be reduced as the water oozes out from the leaf. The THz wave is transmitted through that path, which leads to higher absorptions [23]. Different THz absorption peaks caused by different low temperatures can be considered as the leaf's response to the CI. However, substantial scattering of injured cells in the leaf could result in overlap signals which restrict accurate assessment of damaged cell absorption in the THz region. Therefore, the combination of the THz spectroscopy technique and a mathematical model with chemometrics could provide feasible and effective quantitative assessment of the cold injury in the tea leaves.

THz spectroscopy has been widely employed as a quick and non-destructive method for food- and agricultural-related research. To some extent, valuable information relating to the physiological properties of samples should be able to be efficiently and rapidly extracted from a THz spectral response. Chemometric techniques have been extensively used for processing spectral data to reduce the large number of variations and to sustain process analysis [35]. Chemometric techniques include pre-processing and multivariate analysis of the spectral data. The pre-processing procedures are used to remove irrelevant information and to increase the signal-to-noise ratio. The most common pre-processing methods are the moving average smoothing method and the Savitzky–Golay first and second derivative method [36]. Qualitative classification and quantitative regression are the most common multivariate analysis techniques applied in THz spectroscopy. Among the most commonly used algorithms, partial least squares (PLS) can be effectively combined with another algorithm for model establishment in freezing detection studies [37].

The literature reviewed demonstrates the feasibility of reliance on a THz spectral response to changes in the physiological properties of plant leaves for the assessment of CI. However, only a few research projects concentrated on determining the effectiveness of a THz spectral response to modifications in the macro- and microstructure of plant

tissue during freezing stress in assessing the degree of damage. Therefore, the objectives of this research were as follows: (1) to assess the effect of varying low temperatures applied to tea plants and determine the best THz frequency range of the absorption spectra for the analysis; (2) to combine two-dimensional correlation spectroscopy with partial least square regression (2DCOS–PLSR) to enhance the spectral differences of different low temperatures; and (3) to utilize the correlation intensities obtained from the average spectral and two-dimensional correlation spectroscopy to develop PLSR models and compare their performance for excellent quantitative analysis.

This paper is organized as follows: detailed materials and methods used in the research are presented in Section 2; related results and discussions are provided in Section 3; and the conclusions of the overall paper and future research points are proposed in Section 4.

2. Materials and Methods

2.1. Samples Preparation

The experimental tea farm was in a typical hilly area located along the middle and lower reaches of the Yangtze River (latitude 32°01'37" N, longitude 119°40'17" E). The cultivar of the sampled tea plants was five-year-old Long Jing, which is an early-maturing cultivar and easily suffers from cold injury. Five tea plants, carefully grown in the greenhouse for six weeks, were selected as experimental samples. The goal was to fully stabilize the plants to their original state before the CI detection. The tea leaves were well cleaned twice with distilled water, and any remaining water was blotted with blotting paper before the low-temperature treatment.

2.2. THz Spectra Detection and Assessment of the CI

The laboratory room temperature was around 4.0 °C. The control tea plant was placed into the incubator (MIR253, Sanyo, Japan) after pre-cooling at 4.0 °C for 1 h and reduced further to 0 °C for another 1 h. Subsequently, the initial experimental temperature for the other plant samples was set to 4.0 °C and decreased from 4 °C to the targeted low temperatures of −2.5, −5.0, −7.5, and −10.0 °C, respectively. The initial temperature of 4 °C was to ensure that the leaf's cells were in a uniform state prior to the freezing tests. The setting of the freezing process was as follows: first sample (4.0 and 0 °C); second sample (4.0, 0, and −2.5 °C); third sample (4.0, 0, −2.5, and −5.0 °C); fourth sample (4.0, 0, −2.5, −5.0, and −7.5 °C); fifth sample (4.0, 0, −2.5, −5.0, −7.5, and −10.0 °C). Each temperature was maintained for 1 h. At the end of freezing for each treatment, five top leaves were collected for scanning in the THz time-domain spectral imaging system (TS7400, Advantest, Japan) which was positioned very close to the incubator to avoid disturbance of the CI by the external environment. The scanning chamber had dry air injected into it without interruption throughout the experiment to keep the internal relative humidity (RH) around 2%. The scan measurement area was set to a square of 1.0 cm × 1.0 cm, which included "off" scans (outside the leaf surface) and "on" scans (on the leaf surface). However, the number of "off" and "on" scans depends on the shape and size of the tea leaf. The frequency resolution of TS7400 was set to 1.9 GHz, the dynamic range was set to >50 dB, and the acquisition rate was set to 16 ms/scan. The measurement of the entire sample after different temperatures were applied was carried out under this experimental condition. As shown in Figure 1, THz pulses were transmitted through the leaf sample and generated the corresponding THz time-domain spectra. The latter shows lower amplitude for the sample signal and reaches the detector with a time delay [38–40]. Generally, due to the negative bands and overlaps, data from 0.1–1.6 THz were selected for the quantitative analysis (Figure 1). The data used for the analysis were randomly picked from "on" scan points at every level along the length of the leaf, bringing the number of sampled scan points to ten for each leaf (Table 1). Subsequently, the data acquired from the ten scan points were averaged to ensure that the data used fairly represented the CI of the leaf. THz spectral responses (output) that were used after scanning the leaves included the absorbance as influenced by the CI. The whole process was repeated using new tea plants after freezing.

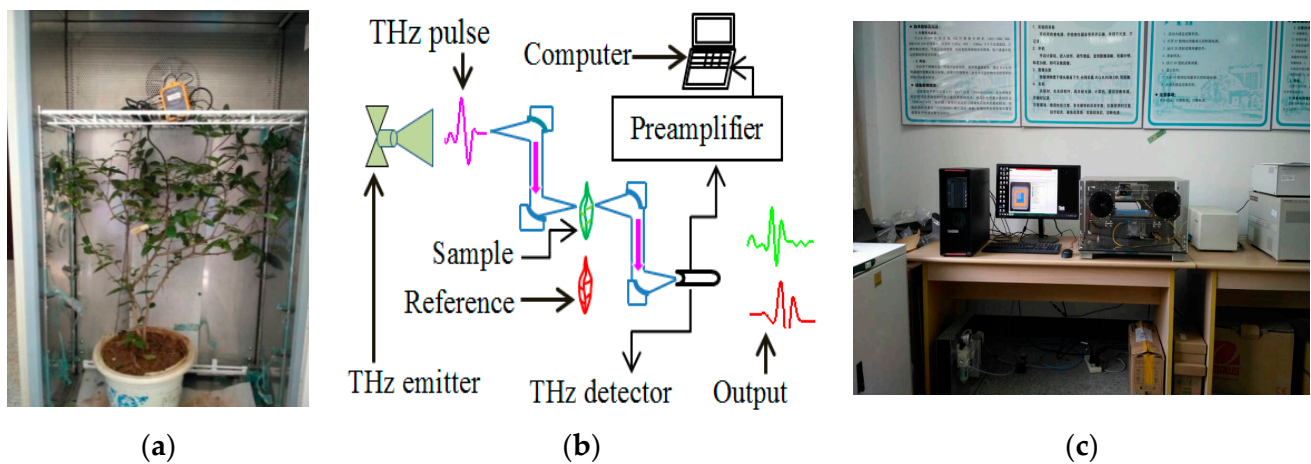


Figure 1. Plant under freezing in the MIR253 (a), spectra measurement with THz-TDS (b), and structure of the THz-TDS system (c).

Table 1. Terahertz spectrum settings for the measurements.

Measurement Types	Dimension Conditions	Dimension Values	
Input dimension parameter of the background measurements	Reference offset (mm)	X	Y
		0.0	0.0
Input dimension parameter of the sample measurements	Scan offset (mm)	X	Y
	Measurement offset (mm)	10.0	10.0
	Coarse measurement step (mm)	1.5	1.5
	Measurement count (mm)	10	10
	Coarse/fine mode	coarse	
Measurement conditions	Frequency resolution (GHz)	3.8	
	Calculated number	32	
	Calculation range start (THz)	0.3	
	Calculation range stop (THz)	4	
	Sample thickness (mm)	1	
	Analysis type	All responses	

2.3. Signal Processing of THz Waveform

THz time-domain spectra were collected in the range of 0.1–1.6 THz. The time-domain spectra were converted to the corresponding frequency-domain spectra by fast Fourier transformation (FFT), which is given by [41]:

$$F(k) = \sum_{i=0}^{N-1} f(n)e^{-j[\frac{2\pi}{N}]nk} \tag{1}$$

$$W_N = e^{-j[\frac{2\pi}{N}]} \tag{2}$$

$$F(k) = \sum_{i=0}^{N-1} f(n)W_N^{nk} (k = 0, 1, \dots, N - 1) \tag{3}$$

where N is the transform size and $f(n)$ is the sequence of the input.

In this study, the FFT function was provided by MATLAB17.0. The FFT obtained the corresponding transformations of these short sequences and made the fitting combination to delete the repeated calculation. In addition to the time-domain spectra, an integer power

of 2 was required as the transform size. Then, based on the general laws of absorption, THz absorbance spectra could be calculated by [42]:

$$\text{Absorbance } (W_t) = \log_{10} \left| \frac{S_s(w_t)}{S_r(w_t)} \right|^2 \quad (4)$$

where $S_s(w_t)$ and $S_r(w_t)$ are the THz components in the frequency domain corresponding to the sample and the condition being studied.

2.4. Computation of 2D Correlation Spectroscopy

It is crucial in modelling to remove the effects of outliers. The leverage–studentized residual method is extensively used to detect the outliers in samples. A studentized residual is the quotient resulting from the ratio of a residual and an estimate of its standard deviation. The responses of samples with high leverage and high studentized residuals were considered outliers [42,43]. The frequently used robust PLSR model was employed to quantitatively analyze the freezing temperature effect on cold injury due to the complexity and high dimension of the THz spectral data [44]. Predictions can be statistically necessary and use the absorbance values within the frequency range 0.1–1.6 THz. Spectrum features were extracted and then the correlation between the instrumental measurements and the values of each predicted property was established [25,45].

Two-dimensional correlation spectroscopy (2DCOS) was utilized to enhance the spectral differences of tea samples held at different low temperatures for different lengths of time. In this study, two-dimensional terahertz correlation spectroscopy (2DCOS–THz) was used to optimize the quantitative analysis model. The 2DCOS–THz technique was achieved by applying stress from different low temperatures on the plants. Subsequently, the THz spectra of the samples were measured and processed by following the generalized two-dimensional (2D) correlation algorithm proposed by Isao Noda [46,47]. For dynamic spectra $\tilde{y}(v, c)$, where v means the frequency and c means the different low temperature, the intensity of a synchronous 2D correlation spectrum $\phi(v_1, v_2)$ represents the simultaneous change of two spectral intensity variations measured at v_1 and v_2 , which is given by the following expression [25,47]:

$$\text{RMSE}_p = \sqrt{\frac{\sum_{i=1}^N (S_{iP} - T_{ir})^2}{N}} \quad (5)$$

Computation of the asynchronous correlation spectrum $\Psi(v_1, v_2)$, which means the out-of-phase or sequential changes of spectral intensity measured at v_1 and v_2 , requires the Hilbert–Noda matrix, defined as [22,45]:

$$N_{jk} = \begin{cases} 0 & j = k \\ \frac{1}{\pi(k-j)} & j \neq k \end{cases} \quad (6)$$

Therefore, N_{jk} is the value in row j and column k of the Hilbert–Noda matrix, and the asynchronous 2D correlation spectrum $\Psi(v_1, v_2)$ is given by the following expression [22,45]:

$$\Psi(v_1, v_2) = \frac{1}{m-1} \sum_{j=1}^m \tilde{y}(v_1) \times N_{jk} \tilde{y}(v_2) \quad (7)$$

2.5. Evaluation of Models' Performance

The correlation coefficient of the prediction set (R_p) and the root mean square error of the prediction set (RMSE_p) were explored to evaluate the prediction precision. They are defined as:

$$R_P = \frac{\sum_{i=1}^N (T_{ir} - \bar{T}_{ir})(S_{ip} - \bar{S}_{ip})}{\sqrt{\sum_{i=1}^N (T_{ir} - \bar{T}_{ir})^2} \sqrt{\sum_{i=1}^N (S_{ip} - \bar{S}_{ip})^2}} \quad (8)$$

$$RMSE_P = \sqrt{\frac{\sum_{i=1}^N (S_{ip} - T_{ir})^2}{N}} \quad (9)$$

where T_{ir} and \bar{T}_{ir} are the reference values of the i^{th} ample and the average values of the reference values, respectively; S_{ip} and \bar{S}_{ip} are the predicted values of the i^{th} sample and the average values of the predicted values, respectively; and N is the number of the samples.

3. Results and Discussion

3.1. Absorbance Response of Tea Leaves to Different Low Temperatures

The trend has shown that seven chief peaks and three subordinate peaks exist in the band. The chief peaks could be found in 0.21 THz, 0.46 THz, 0.62 THz, 0.78 THz, 1.0 THz, 1.32 THz, and 1.54 THz, and the subordinate peaks could be found in 0.32 THz, 0.89 THz, and 1.2 THz (Figure 2).

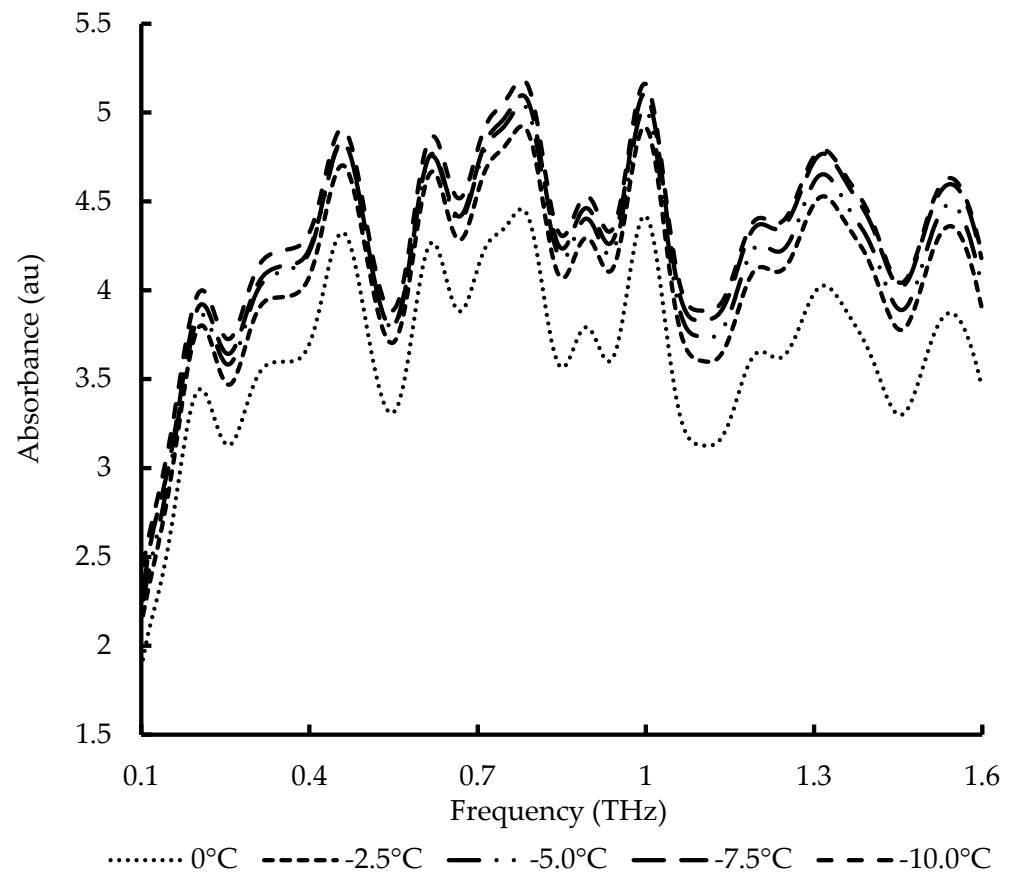


Figure 2. Absorbance spectra in the band of 0.1–1.6 THz of the tea-leaf response to different low temperatures.

The average THz absorbance of tea-plant samples under stress from different low temperatures generally increased significantly with the decrease in temperature. The trend for the temperature of 0 °C was far lower than the trend for the other temperatures and could be easily discriminated. This is because serious injury to tea plants takes place at temperatures below 0 °C. The differences in the absorption peaks for the other temperature levels could not be easily discriminated due to closeness and overlap.

3.2. Multivariate Analysis Using the AI-PLSR and 2DCOS-PLSR Models

3.2.1. The Role of Outliers in the Model

In order to develop a more perfect PLSR model, it is necessary to remove the outliers that may exist in the dataset. In view of this, outliers were detected by calculating the leverage and the studentized residual (Figure 3). Two reference limits of the studentized residual were respectively set to 2 and -2 times the average of the absolute values of all the studentized residuals. Samples that were beyond the reference limit of the studentized residual were judged to be outliers.

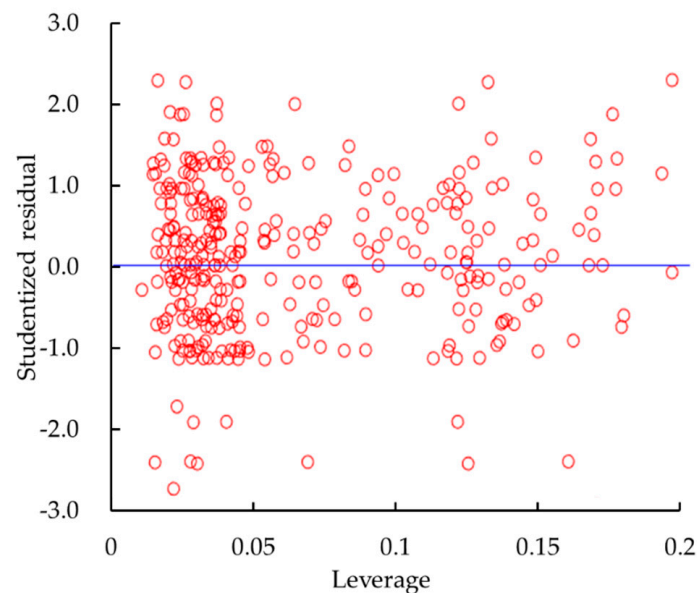


Figure 3. Leverage–studentized residual chart of CI of tea leaves.

3.2.2. Average Intensity (AI) Spectra and Synchronous 2DCOS

The instability features in the absorbance spectrum make it difficult to segregate the absorbance curve changes that result from different temperatures. According to the Lambert–Beer law, absorbance is proportional to the concentrations and thickness of the attenuating species in the material sample. Similarly, the degree of CI which is due to temperature changes is proportional to the absorbance. As a result, the THz spectrum could have more leaf cell openings to interact with at a higher injury level than at a lower injury level. Furthermore, the length of the optical path through which the THz wave is transmitted is reduced at higher injury levels due to the water that oozes out of the leaf [23,32]. The effect is that higher absorptions increase the intensity of cold stress [23]. In this case, the interesting part is the changes in absorbance curves at different low temperatures in a specific frequency range. It is necessary to select the subintervals which contain the most interesting information on CI changes, instead of the whole interval, to reduce the impact of the instability features. The selection of such subintervals could be performed by direct observation. However, the slightest variations could affect robustness and might not be conducive to calculation. Based on the average intensity (AI) spectra (Figure 4), eighteen intervals were selected as follows: 0.168–0.187 THz, 0.351–0.370 THz, 0.450–0.469 THz, 0.530–0.549 THz, 0.626–0.645 THz, 0.729–0.748 THz, 0.824–0.843 THz,

0.866–0.885 THz, 0.938–0.957 THz, 1.030–1.049 THz, 1.072–1.091 THz, 1.137–1.156 THz, 1.194–1.213 THz, 1.251–1.270 THz, 1.385–1.404 THz, 1.461–1.480 THz, 1.530–1.549 THz, and 1.568–1.587 THz.

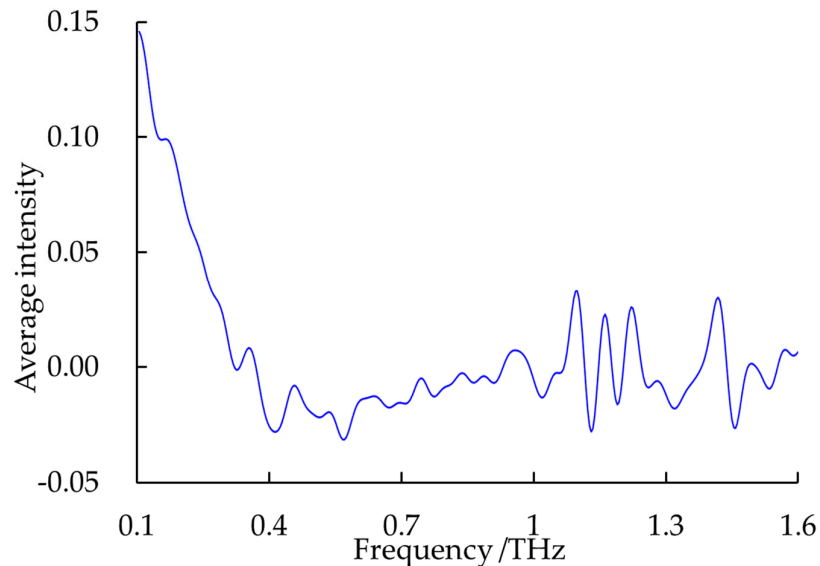


Figure 4. AI of THz absorption spectra din different low temperatures in the range of 0.1–1.6 THz.

Similarly, the necessary enhanced solution was obtained from the synchronous 2D correlation intensity of 2DCOS. Figure 5a presents the 2DCOS–THz synchronous spectra for the THz absorbance of samples at different freezing temperatures. The contours of the temperature-perturbed 2DCOS–THz synchronous spectra reflect the change in the sample’s absorbance. The auto-peak (Figure 5b), which represents the autocorrelation and the vulnerability of perturbation-induced fluctuations of the THz signals, is the diagonal peak of the 2DCOS–THz synchronous spectra. The best input intervals were based on the intensity changes, which are directly correlated to the strength of the peak (Figure 4) as proven by Isao Noda’s study [42]. In this study, fourteen intervals of the frequency were selected as follows: 0.195–0.214 THz, 0.278–0.298 THz, 0.557–0.576 THz, 0.618–0.637 THz, 0.671–0.690 THz, 0.797–0.816 THz, 0.870–0.889 THz, 1.068–1.087 THz, 1.148–1.167 THz, 1.205–1.225 THz, 1.366–1.385 THz, 1.419–1.438 THz, 1.488–1.507 THz, and 1.556–1.575 THz.

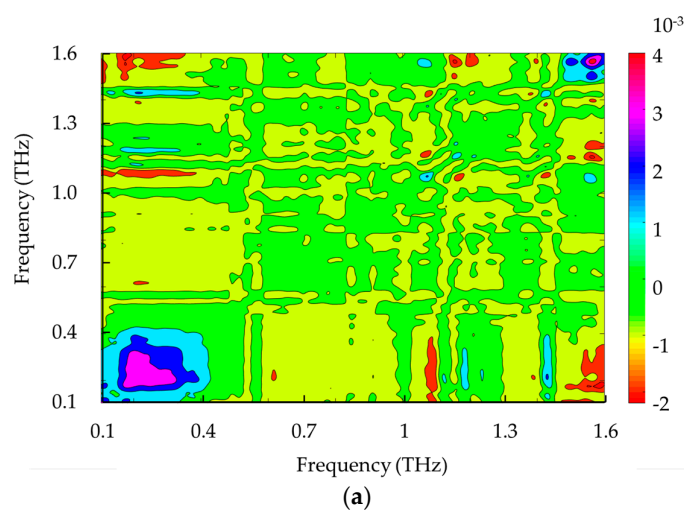


Figure 5. Cont.

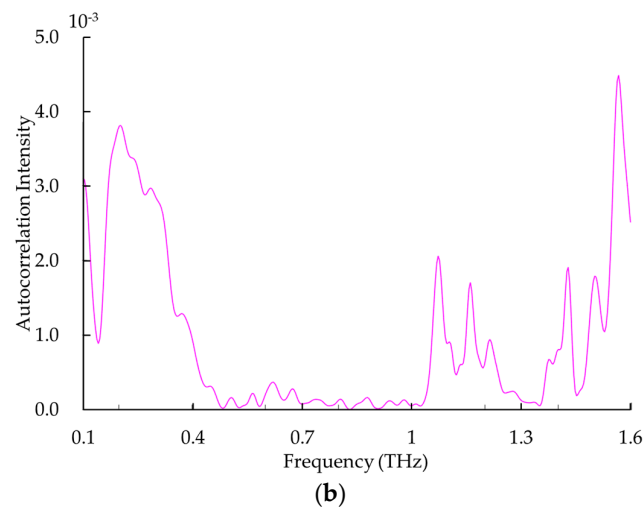


Figure 5. 2DCOS-THz chart in the range between 0.1 THz and 1.6 THz: (a) 2DCOS-THz synchronous spectra; (b) the auto-peaks spectra of CI.

3.2.3. Performance Evaluation of the Models

AI-PLSR models without each outlier were, respectively, built and presented in Table 2. The specific comparisons of the evaluation parameters were the correlation coefficients R_{AI} values and $RMSE_{AI}$ values as shown in Table 2. Compared with the original model, the model of samples without 0 °C-1; −2.5 °C-2; −7.5 °C-1; and −10 °C-1 was more accurate, with an increased value for R_{AI} from 0.7477 to 0.7691 and a decreased value for $RMSE_{AI}$ from 0.6038 to 0.5962. A new model was obtained by removing samples 0 °C-3; −2.5 °C-3; −5 °C-1; −7.5 °C-3 and −10 °C-3. The performance further improved with an increased value for R_{AI} from 0.7691 and 0.8974 and a decreased value for $RMSE_{AI}$ from 0.5962 to 0.5797. This means that the final model is better than the other two described above (Figures 6a, 7a and 8a).

Table 2. Comparison of original PLSR and 2DCOS-PLSR performance.

NO.	Model	R_{AI}	$RMSE_{AI}$	R_{2D}	$RMSE_{2D}$
1	All samples	0.7477	0.6038	0.7873	0.6032
2	Removed, 0 °C-1; −2.5 °C-1; −7.5 °C-1; and −10 °C-1	0.7691	0.5962	0.8305	0.5763
3	Removed, 0 °C-1; −2.5 °C-2; −5 °C-1; −7.5 °C-1 and −10 °C-1	0.8974	0.5797	0.9103	0.5221

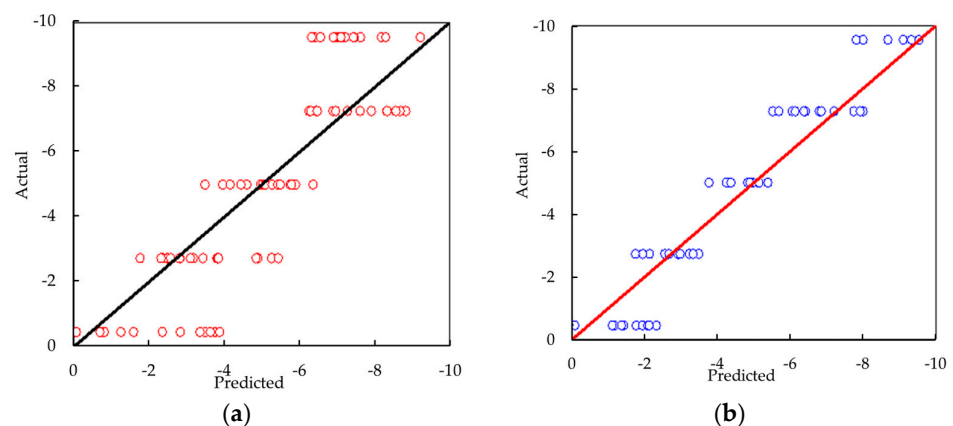


Figure 6. The performance of the models developed with all samples in the form of scatter plots (a) AI-PLSR and (b) 2DCOS-PLSR.

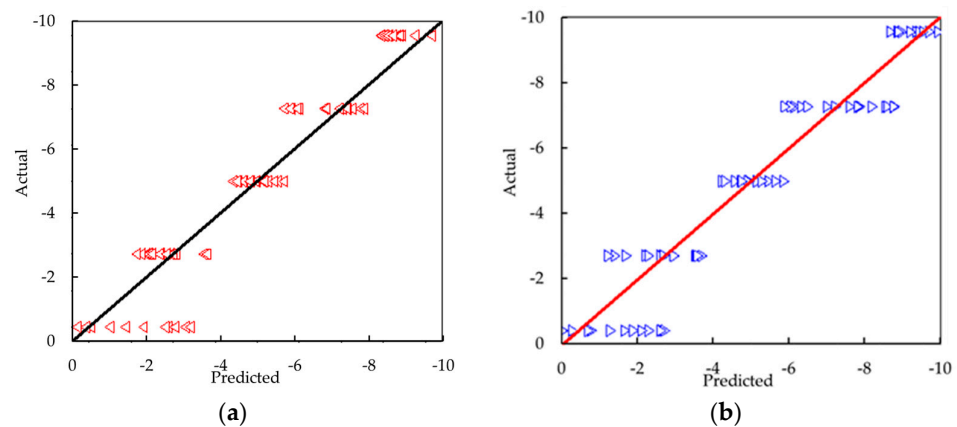


Figure 7. The performance of the models after ($0\text{ }^{\circ}\text{C-1}$; $-2.5\text{ }^{\circ}\text{C-1}$; $-7.5\text{ }^{\circ}\text{C-1}$, and $-10\text{ }^{\circ}\text{C-1}$) were removed in the form of scatter plots (a) AI-PLSR and (b) 2DCOS-PLSR.

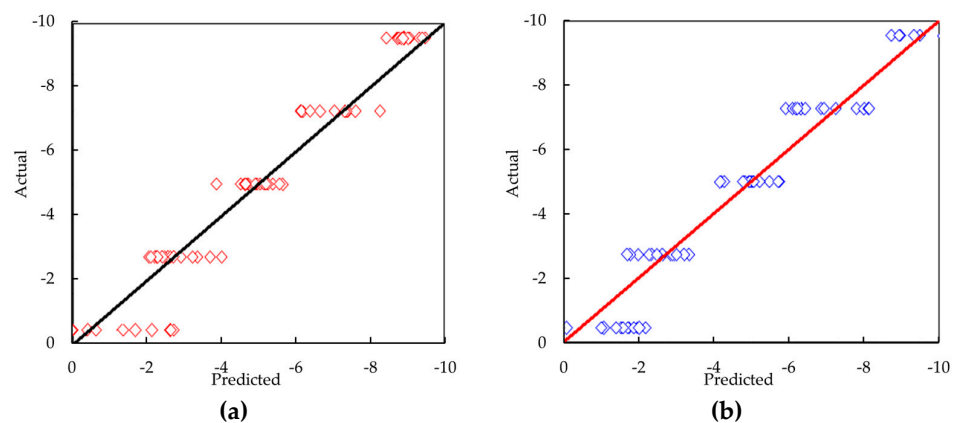


Figure 8. The performance of the models after ($0\text{ }^{\circ}\text{C-1}$; $-2.5\text{ }^{\circ}\text{C-2}$; $-5\text{ }^{\circ}\text{C-1}$; $-7.5\text{ }^{\circ}\text{C-1}$ and $-10\text{ }^{\circ}\text{C-1}$) removed in the form of scatter plots (a) AI-PLSR and (b) 2DCOS-PLSR.

In the same way, models were developed based on 2DCOS, and the scatter distributions of these models are presented in Figures 6b, 7b and 8b. Compared with the first 2DCOS-PLSR model, the model of samples without $0\text{ }^{\circ}\text{C-1}$; $-2.5\text{ }^{\circ}\text{C-2}$; $-7.5\text{ }^{\circ}\text{C-1}$; and $-10\text{ }^{\circ}\text{C-1}$ was more accurate with an increased value for R_{2D} from 0.7873 to 0.8305 and a decreased value for RMSE_{2D} from 0.6032 to 0.5763. The final model performed better than the other two above, with a further increase in the R_{2D} values from 0.8305 to 0.9103 and a decrease in the RMSE_{2D} values from 0.5763 to 0.5221 (Table 2).

The fitting effect between the predicted and the actual values of the scatter distributions for the AI-PLSR model can be ranked as (Figure 8a > Figure 7a > Figure 6a). Subsequently, the 2DCOS-PLSR model indicated that Figure 8b had a higher fitting effect between the predicted and the actual values than Figure 7b, with Figure 6b having the lowest fitting effect. The scatter distributions of the 2DCOS-PLSR model at all levels (Figures 6b, 7b and 8b) had better fitting effect between the predicted and the actual values compared with the AI-PLSR model (Figures 6a, 7a and 8a).

The specific comparisons of the assessment parameters were the correlation coefficient values (R_{AI} and R_{2D}) and the RMSE values (RMSE_{AI} and RMSE_{2D}) as shown in Table 2. THz spectroscopy has the advantage of sensitive discrimination of injured leaf from normal leaf. Therefore, a THz spectra response can be used to provide parameters for the quantitative analysis of cold injury in plant leaves. The 2DCOS-PLSR model had a significant increase in R_{2D} value and a remarkable decrease in RMSE at all the levels. In the quantitative assessment result obtained for the 2DCOS-PLSR model, R_{2D} is 0.7873, 0.8305, and 0.9103, respectively. RMSE_{2D} is 0.6032, 0.5763, and 0.5221, respectively. For the AI-PLSR model, R_{AI}

is 0.7477, 0.7691, and 0.8974, respectively. $RMSE_{AI}$ is 0.6038, 0.5962, and 0.5797, respectively. This shows that the combination of PLSR with 2DCOS provides a better and a clearer benchmark for the input interval selection, and coupled with signal processing it reduces the adverse effect of noisy signals. The excellent performance represents remarkable improvement through the use of 2DCOS–PLSR.

4. Conclusions

In this study, a new method of assessing the CI of a tea cultivar (Long Jing) by measuring the absorption spectra obtained from a non-destructive THz spectroscopy has been established. The study demonstrates the effectiveness of the THz technique in the characterization of the changes associated with cold injury in tea leaves. Though studies have shown that substantial scattering of injured cells in the leaf results in overlap signals which restrict accurate assessment of damaged cell absorption in the THz region, the combination of the THz spectroscopy technique and the 2DCOS–PLSR model with chemometrics has provided feasible and effective quantitative assessment of cold injury in tea leaves.

The fitting effect between the predicted and the actual values of the scatter distributions for the 2DCOS–PLSR model at all levels was significantly higher than for the AI–PLSR model. The 2DCOS–PLSR model had a significantly higher correlation coefficient value and a remarkable decrease in RMSE values at all levels. The combination of PLSR and 2DCOS provided a better and a clearer benchmark for the input interval selection and reduced the adverse effect of noisy signals. The merits of these methods are that they reduce time consumed on repetitive experiments and provide reliable results by decreasing the errors that could be inherited from the operator's skills. The excellent performance represents remarkable improvement through use of the 2DCOS–PLSR model. It is expected that the 2DCOS–PLSR model for the non-destructive evaluation of CI by THz spectroscopy can be further applied in the study of plant nutrients dosage perturbation as part of research into cold tolerance analysis.

In future research, we will evaluate THz spectroscopy and hyperspectral imaging techniques in the detection of freezing injury in other plants that are grown in areas prone to freezing/frost. Further research will also focus on improvements in assessing cold damage and should study temperatures of at least $-15\text{ }^{\circ}\text{C}$ and, if possible, up to $-25\text{ }^{\circ}\text{C}$, since in the plant environment, the plant canopy temperature can sometime decrease to as low as $-30\text{ }^{\circ}\text{C}$. This will ensure that data are made available for all seasons and all regions and for seasonal fluctuations in the ambient temperature.

Author Contributions: Y.L. and E.A.A. conceived and designed the experiments; Y.L. and E.A.A. performed the experiments and analyzed the data; E.A.A. and Y.L. wrote the manuscript; Y.L., Y.H. and H.D. made some helpful comments on how to improve the quality and language of the manuscript. All authors have read and agreed to the published version of the manuscript.

Funding: This research was funded by the China and Jiangsu Postdoctoral Science Foundation (2022M711396 and 2021K614C); the project of the Key Laboratory of Modern Agricultural Equipment and Technology, Jiangsu University (MAET202119); the project of the Jiangsu Province and Education Ministry Co-sponsored Synergistic Innovation Centre of Modern Agricultural Equipment (XTCX2013); the Natural Science Foundation of the Jiangsu Higher Education Institutions of China (21KJB210019); the Postgraduate Innovation Project of Jiangsu Province (KYCX22_3683); and the Academic Programme Development of the Jiangsu Higher Education Institutions (PAPD-2018-87).

Data Availability Statement: Not applicable.

Acknowledgments: We are sincere grateful to the School of Agricultural Engineering, Jiangsu University, for providing all the required instruments without which this work would not have been possible. We would like to express our gratitude to all reviewers for their patience and help.

Conflicts of Interest: The authors declare no conflict of interest.

References

1. Li, X.; Sun, C.; Luo, L.; He, Y. Determination of tea polyphenols content by infrared spectroscopy coupled with iPLS and random frog techniques. *Comput. Electron. Agric.* **2015**, *112*, 28–35. [[CrossRef](#)]
2. Cheng, T.O. Will green tea be even better than black tea to increase coronary flow velocity reserve? *Am. J. Cardiol.* **2004**, *94*, 12–23. [[CrossRef](#)] [[PubMed](#)]
3. Hacker, J.; Ladinig, U.; Wagner, J.; Neuner, G. Inflorescences of alpine cushion plants freeze autonomously and may survive subzero temperatures by super cooling. *Plant Sci.* **2011**, *180*, 149–156. [[CrossRef](#)] [[PubMed](#)]
4. Skupien, J.; Wojtowicz, J.; Kowalewska, L.; Mazur, R.; Garstka, M.; Gieczewska, K.; Mostowska, A. Dark-chilling induces substantial structural changes and modifies galactolipid and carotenoid composition during chloroplast biogenesis in cucumber (*Cucumis sativus* L.) cotyledons. *Plant Physiol. Biochem.* **2017**, *111*, 107–118. [[CrossRef](#)]
5. Asante, E.; Du, Z.; Lu, Y.; Hu, Y. Detection and assessment of nitrogen effect on cold tolerance for tea by hyperspectral reflectance with PLSR, PCR, and LM models. *Inf. Process. Agric.* **2021**, *8*, 96–104. [[CrossRef](#)]
6. Lu, Y.; Hu, Y.; Zhao, C.; Snyder, R.L. Modification of water application rates and intermittent control for sprinkler frost protection. *Trans. ASABE* **2018**, *61*, 1277–1285. [[CrossRef](#)]
7. Lu, Y.; Hu, Y.; Snyder, R.L.; Kent, E.R. Tea leaf's microstructure and ultrastructure response to low temperature in indicating critical damage temperature. *Inf. Process. Agric.* **2019**, *6*, 247–254. [[CrossRef](#)]
8. Hu, Y.; Amoah Asante, E.; Lu, Y.; Mahmood, A.; Ali Buttar, N.; Yuan, S. A review of air disturbance technology for plant frost protection. *Int. J. Agric. Biol. Eng.* **2018**, *11*, 21–28. [[CrossRef](#)]
9. Lu, Y.Z.; Hu, Y.G.; Zhang, X.L.; Li, P.P. Responses of electrical properties of tea leaves to low-temperature stress. *Int. J. Agric. Biol. Eng.* **2015**, *8*, 170–175.
10. Taschler, D.; Neuner, G. Summer frost resistance and freezing patterns measured insitu in leaves of major alpine plant growth forms in relation to their upper distribution boundary. *Plant Cell Environ.* **2004**, *27*, 737–746. [[CrossRef](#)]
11. Skinner, D.Z.; Garland-Campbell, K.A. The relationship of LT50 to prolonged freezing survival in winter wheat. *Can. J. Plant Sci.* **2008**, *88*, 885–889. [[CrossRef](#)]
12. Gusta, L.V.; O'Connor, B.J.; Gao, Y.P.; Jana, S. Are-evaluation of controlled freeze-tests and controlled environment hardening conditions to estimate the winter survival potential of hardy winter wheats. *Can. J. Plant Sci.* **2001**, *81*, 241–246. [[CrossRef](#)]
13. Equiza, M.A.; Francko, D.A. Assessment of freezing injury in palm species by chlorophyll Fluorescence. *HortScience* **2010**, *45*, 845–848. [[CrossRef](#)]
14. Min, K.; Chen, K.; Arora, R. Effect of short-term versus prolonged freezing on freeze–thaw injury and post-thaw recovery in spinach: Importance in laboratory freeze–thaw protocols. *Environ. Exp. Bot.* **2014**, *106*, 124–131. [[CrossRef](#)]
15. Gao, Z.; Li, J.; Zhu, H.; Sun, L.; Du, Y.; Zhai, H. Using differential thermal analysis to analyze cold hardiness in the roots of grape varieties. *Sci. Hort.* **2014**, *174*, 155–163. [[CrossRef](#)]
16. Agarwal, M.; Hao, Y. A R2R3 type MYB3 transcription factor is involved in the cold regulation of CBF genes and in acquired freezing tolerance. *J. Biol. Chem.* **2006**, *281*, 37636–37645. [[CrossRef](#)]
17. Halloy, S.R.P.; Gonzalez, J.A. An inverse relation between frost survival and osmotic pressure. *Arct. Alp. Res.* **1993**, *25*, 117–123. [[CrossRef](#)]
18. Jördens, C.; Scheller, M.; Breitenstein, B.; Selmar, D.; Koch, M. Evaluation of leaf water status by means of permittivity at terahertz frequencies. *J. Biol. Phys.* **2009**, *35*, 255–264. [[CrossRef](#)]
19. Liu, W.; Liu, C.; Hu, X.; Yang, J.; Zheng, L. Application of terahertz spectroscopy imaging for discrimination of transgenic rice seeds with chemometrics. *Food Chem.* **2016**, *210*, 415–421. [[CrossRef](#)]
20. Pan, L.; Zhang, Q.; Zhang, W.; Sun, Y.; Hu, P.; Tu, K. Detection of cold injury in peaches by hyperspectral reflectance imaging and artificial neural network. *Food Chem.* **2016**, *192*, 134–141. [[CrossRef](#)]
21. Wang, K.; Sun, D.W.; Pu, H. Emerging non-destructive terahertz spectroscopic imaging technique: Principle and applications in the agri-food industry. *Trends Food Sci. Technol.* **2017**, *67*, 93–105. [[CrossRef](#)]
22. Mathanker, S.K.; Weckler, P.R.; Wang, N. Terahertz (THz) applications in food and agriculture: A review. *Trans. Am. Soc. Agric. Biol. Eng.* **2013**, *56*, 1213–1226.
23. Walther, M.; Fischer, B.M.; Ortner, A.; Bitzer, A.; Thoman, A.; Helm, H. Chemical sensing and imaging with pulsed terahertz radiation. *Anal. Bioanal. Chem.* **2010**, *397*, 1009–1017. [[CrossRef](#)] [[PubMed](#)]
24. Hadjiloucas, S.; Karatzas, L.S.; Bowen, J.W. Measurements of leaf water content using terahertz radiation. *IEEE Trans. Microw. Theory Tech.* **1999**, *47*, 142–149. [[CrossRef](#)]
25. Wold, S.; Sjostrom, M.; Eriksson, L. PLS-regression: A basic tool of chemometrics. *Chemom. Intell. Lab. Syst.* **2001**, *58*, 109–130. [[CrossRef](#)]
26. Hua, Y.; Zhang, H.; Zhou, H. Quantitative determination of cyfluthrin in Nhexane by Terahertz time-domain spectroscopy with chemometrics methods. *IEEE Trans. Instrum. Meas.* **2010**, *59*, 1414–1423.
27. Suzuki, T.; Ogawa, Y.; Kondo, N. Characterization of pesticide residue, cis-permethrin by terahertz spectroscopy, Engineering in Agriculture. *Environ. Food* **2011**, *4*, 90–94.
28. Zhao, X.L.; Li, J.S. Diagnostic techniques of talc powder in flour based on the THz spectroscopy. *J. Phys. Conf. Ser.* **2011**, *276*. [[CrossRef](#)]

29. Chen, T.; Li, Z.; Yin, X.; Hu, F.; Hu, C. Discrimination of genetically modified sugar beets based on terahertz spectroscopy. *Spectrochim. Acta Part A Mol. Biomol.* **2016**, *153*, 586–590. [[CrossRef](#)]
30. Lu, Y.Z.; Hu, Y.G.; Li, P.P. Consistency of electrical and physiological properties of tea leaves on indicating critical cold temperature. *Biosyst. Eng.* **2017**, *159*, 89–96. [[CrossRef](#)]
31. Chan, W.L.; Deibel, J.; Mittleman, D.M. Imaging with terahertz radiation. *Rep. Prog. Phys.* **2007**, *70*, 1325–1379. [[CrossRef](#)]
32. Lourenço, N.D.; Lopes, J.A.; Almeida, C.F.; Sarraguça, M.C.; Pinheiro, H.M. Bioreactor monitoring with spectroscopy and chemometrics: A review. *Anal. Bioanal. Chem.* **2012**, *404*, 1211–1237. [[CrossRef](#)]
33. Castro-camus, E.; Palomar, M.; Covarrubias, A.A. Leaf water dynamics of *Arabidopsis thaliana* monitored in vivo using terahertz time-domain spectroscopy. *Sci. Rep.* **2013**, *3*, 2910. [[CrossRef](#)]
34. Born, N.; Behringer, D.; Liepelt, S.; Beyer, S.; Schwerdtfeger, M.; Ziegenhagen, B.; Koch, M. Monitoring Plant Drought Stress Response Using Terahertz Time-Domain Spectroscopy. *Plant Physiol.* **2014**, *164*, 1571–1577. [[CrossRef](#)]
35. Suhandy, D.; Yulia, M.; Ogawa, Y.; Kondo, N. Prediction of L-Ascorbic Acid using FTIR-ATR Terahertz Spectroscopy Combined with Interval Partial Least Squares (iPLS) Regression. *Eng. Agric. Environ. Food* **2013**, *6*, 111–117. [[CrossRef](#)]
36. Pan, T.T.; Sun, D.W.; Cheng, J.H.; Pu, H. Regression algorithms in hyperspectral data analysis for meat quality detection and evaluation. *Compr. Rev. Food Sci. Food Saf.* **2016**, *15*, 529–541. [[CrossRef](#)]
37. Zhang, X.C.; Xu, J. THz spectroscopy and imaging. In *Introduction to THz Wave Photonics*; Springer: New York, NY, USA, 2010; pp. 49–69.
38. Zhang, H.; Zhi Li, Z.; Tao, T.; Qin, B. Quantitative determination of Auramine O by terahertz spectroscopy with 2DCOS-PLSR model. *Spectrochim. Acta Part A Mol. Biomol. Spectrosc.* **2017**, *184*, 335–341. [[CrossRef](#)]
39. Song, F.V.; Yang, B.; Di Tommaso, D.; Donnan, R.S.; Chass, G.A.; Yada, R.Y.; Farrar, D.H.; Tian, K.V. Resolving nanoscopic structuring and interfacial THz dynamics in setting cements. *Mater. Adv.* **2022**, *3*, 4982–4990. [[CrossRef](#)]
40. Tian, K.V.; Yang, B.; Yue, Y.; Bowron, D.T.; Mayers, J.; Donnan, R.S.; Dobó-Nagy, C.; Nicholson, J.W.; Fang, D.-C.; Greer, A.L.; et al. Atomic and vibrational origins of mechanical toughness in bioactive cement during setting. *Nat. Commun.* **2015**, *6*, 8631. [[CrossRef](#)]
41. Heideman, M.T.; Johnson, D.H.; Burrus, C.S. “Gauss and the history of the fast Fourier transform” (PDF). *IEEE ASSP Mag.* **1984**, *1*, 14–21. [[CrossRef](#)]
42. Pedro, A.M.K.; Ferreira, M.M.C. Nondestructive Determination of Solids and Carotenoids in Tomato Products by Near-Infrared Spectroscopy and Multivariate Calibration. *Anal. Chem.* **2005**, *77*, 2505–2511. [[CrossRef](#)] [[PubMed](#)]
43. Mazarevica, G.; Diewok, J.; Baena, J.; Rosenberg, E.; Lendl, B. On-line fermentation monitoring by mid-infrared spectroscopy. *Appl. Spectrosc.* **2004**, *58*, 804–810. [[CrossRef](#)] [[PubMed](#)]
44. Groberio, T.S.; Zacca, J.J.; Talhavini, M.; Braga, J.W.B. Quantification of cocaine hydrochloride in seized drug samples by infrared spectroscopy and PLSR. *J. Braz. Chem. Soc.* **2014**, *25*, 1696–1703. [[CrossRef](#)]
45. Noda, I. Techniques useful in two-dimensional correlation and codistribution spectroscopy (2DCOS and 2DCDS) analyses. *J. Mol. Struct.* **2016**, *1124*, 29–41. [[CrossRef](#)]
46. Noda, I. Generalized 2-dimensional correlation method applicable to infrared, raman, and other types of spectroscopy. *Appl. Spectrosc.* **1993**, *47*, 1329–1336. [[CrossRef](#)]
47. Noda, I. Determination of two-dimensional correlation spectra using the Hilbert transform. *Appl. Spectrosc.* **2000**, *54*, 994–999. [[CrossRef](#)]

Disclaimer/Publisher’s Note: The statements, opinions and data contained in all publications are solely those of the individual author(s) and contributor(s) and not of MDPI and/or the editor(s). MDPI and/or the editor(s) disclaim responsibility for any injury to people or property resulting from any ideas, methods, instructions or products referred to in the content.